This article has been accepted for publication in IEEE Transactions on Intelligent Transportation Systems. This is the author's version which has not been fully edited and content may change prior to final publication. Citation information: DOI: 10.1109/TITS.2022.3183204

Modeling Driving Behavior of Human Drivers for Trajectory Planning

Christoph Ziegler, Volker Willert and Jürgen Adamy

***Abstract*—Extracted driving behavior of human driven vehicles can benefit the development of various applications like trajectory prediction or planning, abnormal driving detection, driving behavior classification, traffic simulation modeling, etc. In this paper, we focus on modeling human driving behavior in order to find simplifications for trajectory planning. Using a time-discrete kinematic bicycle model with the vehicle's acceleration and steering rate as inputs, we model the human driven trajectories of an urban intersection drone dataset for different input sampling times. While most planning algorithms are using input sampling times below 0.33 s, we are able to model 98.2 % of the human driven trajectories of the investigated dataset with a sampling time of 0.6 s. Using longer input sampling times can result in smoother trajectories and longer planning horizons, and thus more efficient trajectories. In a next step, we analyze the correlations between the input of our model and the current state/last input. Such a priori knowledge could simplify common planning algorithms like model predictive control or tree-search based planners by limiting the action space of the ego-vehicle. We propose nonlinear transformations for steering rate and steering angle to represent correlations between speed, acceleration, steering angle and steering rate. In the transformed space the statistics are very well modeled by multivariate Gaussian distributions. Using a multivariate Gaussian, a fast usable behavior model is extracted which is independent of the environment.**

***Index Terms*—Driving behavior, sampling time, sampling rate, automated vehicles, kinematic bicycle model, statistics, trajectory planning, urban driving.**

I. Introduction

Intelligent vehicles are a key component for the traffic of today and the future. Understanding and modeling human driving behavior can benefit the research and automotive industry to improve such vehicles in various aspects. For autonomous driving applications or advanced driver assistance systems, knowledge of driving behavior helps the development of intelligent systems or related tools (e. g. traffic simulator). Fig. 1 shows an exemplary trajectory of a human driver performing a right turn at an inner city intersection. The key question here is how this and other trajectories of other traffic participants can be represented in order to achieve a simple yet accurate model of an average human driver.

The human driving behavior varies and depends on numerous factors such as the driver's skill and mood, the driven vehicle, the culture, the current traffic flow and situation, the weather conditions, etc. [2]. To improve safety functions, a lot of research is focusing on the classification of discrete motion models [3], [4] and driving styles (e. g. calm/aggressive) [5]–[8]. Such knowledge can be used to e. g. detect risky behavior of the current driver [9], [10]. While for such application it is beneficial to distinguish between different driver models, other applications (e. g. trajectory planning) prefer a universal driver model.

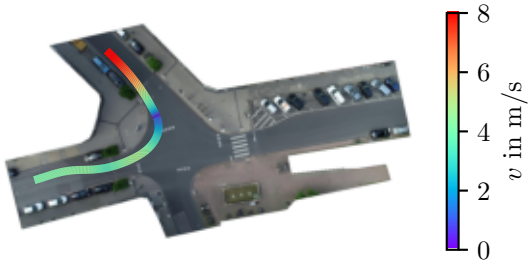

Fig. 1: Exemplary trajectory (path and speed) of a human driver at an inner city intersection. How can this trajectory be approximated and simplified in order to utilize simpler planning? Data taken from the inD dataset [1] (recording 28, track 64).

Calculating a safe, comfortable, ecological and feasible trajectory for an autonomous vehicle is one of the key elements to establish autonomous driving in the future. Especially in urban areas, for the task of trajectory planning, it is important to look ahead, anticipate other traffic participants and plan in a human-like fashion [11]. In order to plan human-like trajectories, cost functions of the planning algorithm can be learned from naturalistic human driving data [12], [13]. In 1985, Reif and Sharir [14] already analyzed the computational complexity of a trajectory planning problem with moving objects and proved that it is PSPACE-hard. Since this complex task is not easy to solve, especially in real time, the idea is to limit the action space of the autonomous vehicle during the planning phase before the cost function is applied. Here, physical limits of the vehicle as well as average human driving behavior can be used to decrease the search space of the planner.

In this paper, we combine the physical and human aspects for planning limitations. For the physical part, the kinematic bicycle model is used to represent the non-holonomic movements of a car-like vehicle. Adding a probabilistic behavioral model on top, the correlations between human actions and their vehicle's states can be taken into account. With this, human driving behavior can be considered by limiting the inputs of the kinematic model. In order to obtain an environmental independent model, we solely consider the trajectories of each human driven vehicle separately without the surrounding road layout or traffic participants. We choose to extract an environmental independent model, since in urban

This work was supported by Continental AG. *(Corresponding author: Christoph Ziegler.)*

Christoph Ziegler and Jürgen Adamy are with the Control Methods and Robotics Lab at Technical University of Darmstadt, Landgraf-Georg-Straße 4, 64283 Darmstadt, Germany (e-mail: christoph.ziegler@rmr.tu-darmstadt.de; adamy@rmr.tu-darmstadt.de).

Volker Willert is with the Faculty of Electrical Engineering at University of Applied Sciences Würzburg-Schweinfurt, Konrad-Geiger-Straße 2, 97421 Schweinfurt, Germany (e-mail: volker.willert@fhws.de).

This article has been accepted for publication in IEEE Transactions on Intelligent Transportation Systems. This is the author's version which has not been fully edited and content may change prior to final publication. Citation information: DOI: 10.1109/TITS.2022.3183204

environments the number of possible situations and maneuvers is so high that it is not possible to define and model all of them with respect to the environment. Furthermore, to benefit the complex task of planning, the model should be fast as it must be executed often. Our extracted model can then be used in various trajectory planning algorithms, e. g. in a stochastic model predictive controller. For an overview of planning algorithms, the reader is referred to [15]. Since our area of application is trajectory planning, the focus of this paper will be put on this topic, but the results presented here can also be used in other applications.

A. Related Work

In the field of driving behavior models, most work focuses on the classification of discrete driving styles [5]–[8]. Since we are not interested in such discrete classifications, the focus below is on continuous behavior models. In general, the acceleration/deceleration (A/D) behavior of human driven vehicles is often analyzed. Bokare and Maurya [16] model the A/D behavior of multiple vehicle classes in India by placing GPS-sensors on the vehicles. Through observation of experiments on straight roads, they found out that for trucks, diesel and petrol cars the acceleration depends exponentially on the speed while for the deceleration there is no statistically significance between an exponential and polynomial model. Other work like Miyajima et al. [17] model the longitudinal driving behavior with a Gaussian Mixture Model for gas and brake pedal commands in order to identify the driver of the vehicle. Wagner et al. [18] analyze the longitudinal motion of car-following scenarios. Using the statistical measure of the maximal information content, they found the dominant correlation between the speed and distance to the vehicle in front.

In the above mentioned work, only the longitudinal behavior of vehicles is analyzed. The lateral movements (i. e. steering) can also be taken into account. In Miyajima's et al. [19] work, the driver's actions are categorized in risk groups based on the acceleration, deceleration and steering of the vehicle. Utilizing the knowledge of experts, three models (A/D and steering) are derived to categorize risky driving behavior. Yokoyama and Toyoda [10] analyzed the correlation between accidents and driving behavior in a long-term study. In their work, A/D and steering is again taken into account to improve the result of their model. For all of the above mentioned literature, an application specific classifier (e. g. risky behavior detection) is the output of the derived model.

In the field of trajectory planning, data driven models are a common choice as well. Here, the output can e. g. be a cost function [13] or uncertainty based trajectories [20]. Using deep-learning methods, Schulz et al. [21] derive an interaction-aware probabilistic Markovian behavior model in order to calculate Gaussian distributions of the next acceleration and steering angle of the ego-vehicle dependent on the current traffic situation. While the idea behind this model is similar to our approach, it incorporates environmental data like the road-layout and the state of other traffic participants. In contrast to Schulz et al., our environment free model of an average driver focuses on the internal states of the vehicle, uses the acceleration and steering velocity as inputs and, because of its simplicity, can be used as basis for further, more complex approaches. Since no deep-learning methods are used, we can rely purely on measured data and do not need to incorporate artificially created data like in [21]. Our model can either be used directly or, for specific applications like a safety check for planned trajectories, the action limits can be extracted.

B. Paper Overview

The remainder of this paper is organized as follows: We first introduce the kinematic bicycle model in Sec. II, which is the basic movement model of a non-holonomic vehicle which we use in our further examinations. In Sec. III we analyze the input sampling time T of the time-discrete bicycle model in order to appropriately describe the movements of human drivers in a publicly available dataset. Finally, an environmental independent behavioral model is presented in Sec. IV before concluding the paper in Sec. V.

II. Kinematic Bicycle Model

The kinematic bicycle model [22] is a simple but accurate vehicle model which describes the non-holonomic movements of a car-like, front-steered vehicle. It is well established in the trajectory planning community and is a common choice e. g. when planning with model predictive control [23]. Furthermore, Polack et al. [24] presented that by limiting the lateral acceleration to $0.54\mu g$, the kinematic bicycle model approximates the movement of a real vehicle sufficiently. Thus, realistic physical planning with the bicycle model is possible.

A. The Standard Bicycle Model

In the following, the kinematic bicycle model is shortly presented. It consists of the state vector $\boldsymbol{x}_\mathrm{s} = [{}_\mathrm{E}x_\mathrm{ref},\, {}_\mathrm{E}y_\mathrm{ref},\, \psi]^\mathrm{T}$ which describes the pose of the vehicle in an earth-fixed coordinate system ${}_\mathrm{E}\mathcal{F}$. The input vector is $\boldsymbol{u}_\mathrm{s} = [v, \delta]^\mathrm{T}$, whereas

${}_\mathrm{E}x_\mathrm{ref}$, ${}_\mathrm{E}y_\mathrm{ref}$: position of the reference point in a given earth coordinate frame,
ψ : orientation of the vehicle,
v : speed of the vehicle,
δ : front wheel steering angle of the vehicle.

Further parameters of the model are

l : wheelbase,
l_ref : length between rear axle and reference point,
β : sideslip angle.

The sideslip angle β is defined as the direction of movement relative to the vehicle's orientation ψ. A visualization of the bicycle model's states and parameters are given in Fig. 2.

This article has been accepted for publication in IEEE Transactions on Intelligent Transportation Systems. This is the author's version which has not been fully edited and content may change prior to final publication. Citation information: DOI: 10.1109/TITS.2022.3183204

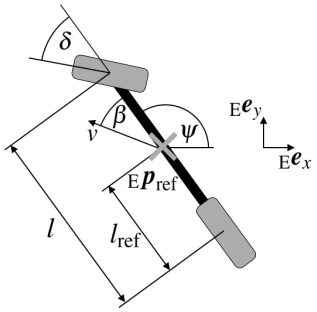

Fig. 2: Definition of states and parameters in the bicycle model.

For $l_{\text{ref}} > 0$, the motion of the vehicle is described by the following non-linear ordinary differential equation (ODE)

$$ {}_{\text{E}}\dot{x}_{\text{ref}} = v\cos(\psi+\beta), \tag{1} $$

$$ {}_{\text{E}}\dot{y}_{\text{ref}} = v\sin(\psi+\beta), \tag{2} $$

$$ \dot{\psi} = \frac{v\cos\beta\tan\delta}{l}, \tag{3} $$

with

$$ \beta = \arctan\left(\frac{l_{\text{ref}}\tan\delta}{l}\right). \tag{4} $$

The model assumes that the vehicle drives slip free (cf. (4)), so the input of the model can either consist of the steering angle δ or the sideslip angle β. From the sideslip angle, the instantaneous curvature κ of the reference point's driven path is derived:

$$ \kappa = \frac{\sin(\beta)}{l_{\text{ref}}}. \tag{5} $$

Most trajectories are planned in a time-discrete fashion, i. e. constant inputs between two discrete time points. For such inputs, the resulting vehicle's driven path consists of partially constant curvatures. For larger input sampling times T_{in} of the time-discrete model, it is harder to follow the resulting unsteady paths. This is why the presented standard model is extended in the following section.

B. Extension of the Bicycle Model

To smoothen the calculated trajectory for a partially constant input $\boldsymbol{u}$, the input of the model is changed to the derivative of the standard one. Therefore, the new input vector is defined as $\boldsymbol{u} = [a, \omega]^{\text{T}}$ with

a : acceleration of the vehicle,

ω : front wheel steering rate.

and the state vector is extended to $\boldsymbol{x} = [{}_{\text{E}}x_{\text{ref}}, {}_{\text{E}}y_{\text{ref}}, \psi, v, \delta]^{\text{T}}$. This results in the following differential equations:

$$ {}_{\text{E}}\dot{x}_{\text{ref}} = v\cos(\psi+\beta), \tag{6} $$

$$ {}_{\text{E}}\dot{y}_{\text{ref}} = v\sin(\psi+\beta), \tag{7} $$

$$ \dot{\psi} = \frac{v\cos\beta\tan\delta}{l}, \tag{8} $$

$$ \dot{v} = a, \tag{9} $$

$$ \dot{\delta} = \omega, \tag{10} $$

with

$$ \beta = \arctan\left(\frac{l_{\text{ref}}\tan\delta}{l}\right). \tag{11} $$

While the idea of extending the bicycle model already exists in the literature (e. g. trajectory tracking controller with jerk and steering velocity as inputs [25]), we want to emphasize the importance of this extension. The sideslip angle β now changes during a constant input $\boldsymbol{u}$, resulting in non-constant instantaneous curvatures. This enables the use of longer sampling times as analyzed in the next section.

III. Input Sampling time of human drivers

Most planning algorithms are calculating trajectories with discrete-time inputs. This means, that the input of the continuous models of Sec. II can only change after a set time, the input sampling time T_{in}. The question now arises which input sampling time can be used to reproduce human driven trajectories like the one in Fig. 1.

By using a larger input sampling time, the planning problem can be simplified since the next action needs to be calculated less often. Thus, using the same computational effort, longer trajectories can be calculated. This can also result in smoother trajectories with fewer high frequency oscillations, especially when using derivatives as an input like in the extended bicycle model of Sec. II-B. However, when the input sampling time is too large, the resulting trajectory is too inflexible in order to handle all required traffic scenarios. Therefore, a trade-off between simplicity of the planning problem and flexibility of the result set needs to be made.

At this point, we want to distinguish between the input sampling time T_{in} and the refresh time t_{refresh} of a planning algorithm. The refresh time is defined as the time between the last and the next planned trajectory. In contrast to the sampling time, which limits the state space, the refresh time mainly influences the ability to react to other dynamic objects in the environment. Both can be chosen independently of each other, even though some algorithms can reuse intermediate calculations if $t_{\text{refresh}} = T_{\text{in}}$ (e. g. in search-trees). Therefore, if the refresh time is chosen accordingly, a large input sampling time T_{in} does not result in the inability to react to time-critical maneuvers.

In the following, we first present sampling times chosen in the literature before analyzing the sampling time of human drivers in urban scenarios.

A. Input Sampling Times in the Literature

To the best of the authors' knowledge, there is no publication which discusses the choice of input sampling time of human trajectories.

In planning, most publications focus on their concept of solving the planning problem and mention their chosen sampling time during the experiment description. Since we analyze the sampling time, we neglect path planning approaches, which optimize the velocity over the planned path in a second step. In most of these approaches, a sampling distance for the path planning is only mentioned. Tab. I shows the input sampling time of recently published trajectory planners. Here, the longest sampling time is 0.333 s.

This article has been accepted for publication in IEEE Transactions on Intelligent Transportation Systems. This is the author's version which has not been fully edited and content may change prior to final publication. Citation information: DOI: 10.1109/TITS.2022.3183204

TABLE I: Common values of the input sampling time T_{in} for trajectory planning algorithms in the literature.

Reference	Model	T_{in} in s
Seccamonte et al. [23]	MPC, bicycle model dependent on κ	0.05
Dixit et al. [26]	MPC, bicycle model with acceleration	0.1
Gutjahr et al. [27]	MPC, linear bicycle model	0.2
Ziegler et al. [28]	Jerk free, continuous optimization	0.333

B. Analysis of the Input Sampling Time of Human Drivers

In order to analyze the input sampling time for human drivers in urban scenarios, we use the drone dataset inD [1] which captures trajectories of trucks, cars, bicycles and pedestrians at four different intersections located in Aachen, Germany. For each vehicle and time step, the dataset contains extracted information like the vehicle's pose in an earth-fixed local coordinate system, the vehicle's velocity, acceleration and extent. Since the trajectory data is derived from drone images, the data does not include information about the vehicle's steering angle. As any real-world dataset, it contains measurement noise but according to [1] the positioning error is typically less than 0.1 m. The dataset is divided in 33 different recordings, each recorded with a frequency of 25 Hz and time lengths between 20-22 minutes. For all recordings, we observe the trajectories of 7326 vehicles which results in $\sim$2.5 Mio. data points. In the following we refer to this dataset as ground truth data. For the analysis of the input sampling time, we proceed as follows: First, the extended bicycle model of Sec. II-B is fitted into the measurement data for different input sampling times. Then, the result is interpreted.

To fit the data, we formulate the following constrained optimization problem. Solving the continuous equations of (6)-(11) with the Runge-Kutta method of fourth order in 25 Hz, we receive m vehicle states for each input $\boldsymbol{u}_k$ with $m = T_{\text{in}} \cdot 25\,\text{Hz}$. For each time-discrete action $\boldsymbol{u}_k$, the mean of the m squared Euclidean distances between the position of the fitted bicycle model ${}_{\text{E}}\boldsymbol{x}_{\text{ref,bm}}$ and of the inD dataset ${}_{\text{E}}\boldsymbol{x}_{\text{ref,inD}}$ is minimized:

$$\min_{\boldsymbol{u}_k} J(\boldsymbol{u}_k) = \sum_{k=0}^{h} \frac{1}{m} \sum_{n=0}^{m} \left\| \begin{bmatrix} {}_{\text{E}}x_{\text{ref,bm}}(\boldsymbol{u}_k, n) \\ {}_{\text{E}}y_{\text{ref,bm}}(\boldsymbol{u}_k, n) \end{bmatrix} - \begin{bmatrix} {}_{\text{E}}x_{\text{ref,inD}}(n+mk) \\ {}_{\text{E}}y_{\text{ref,inD}}(n+mk) \end{bmatrix} \right\|_2^2 \tag{12}$$

$$\text{subject to} \quad v \geq 0, \tag{13}$$

$$-6\,\text{m}\,\text{s}^{-2} < a_k \leq 6\,\text{m}\,\text{s}^{-2}, \tag{14}$$

$$-\arcsin(\kappa_{\max} l) \leq \delta_k \leq \arcsin(\kappa_{\max} l), \tag{15}$$

$$-\pi\,\text{rad}\,\text{s}^{-1} \leq \omega_k \leq \pi\,\text{rad}\,\text{s}^{-1}, \tag{16}$$

$$(6) - (11). \tag{17}$$

The maximum drivable curvature is defined to $\kappa_{\max} = 0.2\,\text{m}^{-1}$, which is a typical value for a small-sized car. Since $\kappa_{\max}$ only decreases for larger vehicles, we assume this as a valid upper limit. The optimization starts using the first value of the ground truth data and is solved until the end of the trajectory T_h is reached.

Since the dataset only includes the length l_{total} from the front to the back of the extracted vehicles but not the wheelbase l, 37 vehicles of various brands and vehicle classes are analyzed. From this, we assume the wheelbase l to be 60 % of the extracted vehicle length l_{total} and the position of the reference point l_{ref} is located at 28.9 % of the wheelbase. Limiting the input and states of the bicycle model during optimization, we assure that the corresponding movement of the vehicle is physically feasible. Furthermore, in (12) only the positional error of the vehicles is minimized for each time step n since adding more terms (e. g. speed, orientation) to the cost function decreased the convergence. With this cost function, the speed of the vehicle is indirectly included due to the time dependency.

TABLE II: Percentage of failed trajectories of the 7326 trajectories as well as the mean and standard deviation of the distance d of the fitted bicycle model to the ground truth data dependent on different input sampling times T_{in}. A trajectory is considered as failed if the Euclidean distance d of one optimized trajectory point to the corresponding ground truth point is larger than 0.3 m.

T_{in}	0.2 s	0.4 s	0.6 s	0.8 s	1.0 s
Failed	0.3 %	0.1 %	1.8 %	5.5 %	11.6 %
Mean(d)	6 mm	6 mm	13 mm	26 mm	49 mm
Std(d)	0.12 mm	0.02 mm	0.02 mm	0.04 mm	0.20 mm

In order to analyze the result of the optimization problem in regard of different sampling times, the optimization results are taken in the frequency of the ground truth data (25 Hz). An optimization is declared as failed if the distance between any points of the optimization result and the corresponding ground truth point is larger than 0.3 m. With this limit, we consider the measurement noise of the dataset and are still able to be close to the original trajectory.

For a first analysis, consider again the trajectory presented in Fig. 1. Here, the driver shortly stops before driving into the intersection and performs a right turn. Fig. 3 shows the results of the optimization problem. For different sampling times T_{in} between 0.2 s and 1.0 s, the traveled distance s, the speed v as well as the Euclidean distance d to the ground truth data are plotted. If the sampling time T_{in} is chosen too large, the optimized trajectory begins to oscillate around the ground truth trajectory and thus periodically increasing and decreasing the error d. For larger sampling times, the effect of oscillation increases and eventually leads to failed optimizations.

In Tab. II the results of all optimized trajectories for different input sampling times between 0.2 s and 1.0 s are shown. By increasing the sampling time T_{in}, the number of failed trajectories and the mean and standard deviation of the positional error increase as well. This can be explained with the above shown increase of oscillating error d of the optimized trajectory. Choosing a sampling time larger than 0.6 s, the number of failed trajectories reaches the 5 % mark. We interpret these sampling times with our chosen kinematic model as being too large to generalize human driving and thus propose to choose the sampling time less or equal to 0.6 s. For this sampling time the oscillation of the optimized trajectory is still acceptable.

To further demonstrate the use of our results on trajectory planners, we implemented a vanilla tree-search trajectory planner based on the extended kinematic bicycle model (cf. (6) – (11)). For each planning step, the planner can choose between 7 different steering rates. As objective function, the lateral distance and orientation difference to the center line as well as the Euclidean distance to other objects are chosen. In Fig. 4, an exemplary overtaking scenario of a parked vehicle

This article has been accepted for publication in IEEE Transactions on Intelligent Transportation Systems. This is the author's version which has not been fully edited and content may change prior to final publication. Citation information: DOI: 10.1109/TITS.2022.3183204

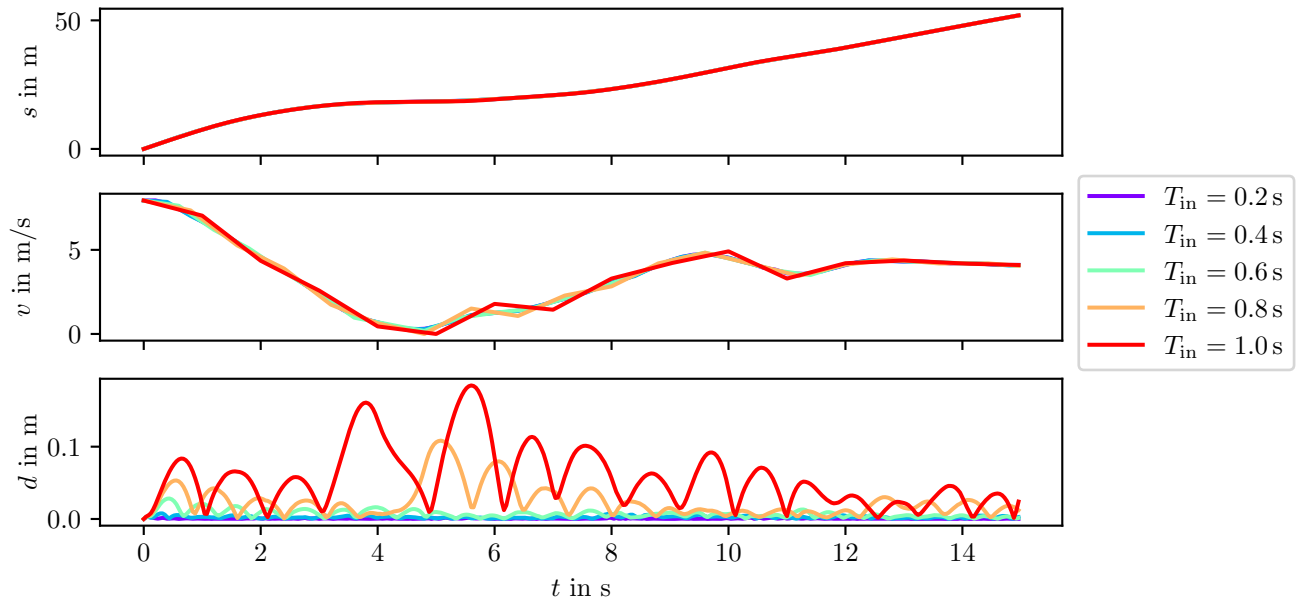

Fig. 3: Optimization result for different input sampling times T_{in} for one exemplary trajectory (recording 28, track 64). The traveled distance s, the speed v and the Euclidean distance to the ground truth data d are plotted. Increasing T_{in} results in a less flexible trajectory. If T_{in} is chosen too large, the optimized trajectory will oscillate around the ground truth trajectory resulting in periodically changing errors d.

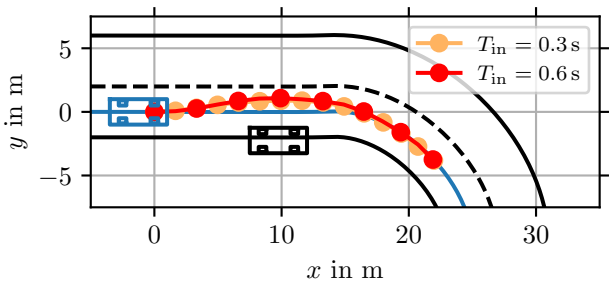

Fig. 4: Two planned trajectories for the ego vehicle (blue) with different input sampling times. The vehicle tries to follow the center line of the road (blue) while keeping a safe distance to the parked vehicle (black). Even though the sampling time T_{in} of the red trajectory is doubled compared to the orange one, the planned trajectory is almost the same.

is shown. Two trajectories were planned using the sampling times $T_{in} = 0.3\,s$ (orange) and $T_{in} = 0.6\,s$ (red). The planned trajectories differ only slightly, although the sampling time has been doubled.

IV. Behavior Model of Human Drivers

A behavior model describes possible movements of a vehicle dependent on its current state. Such a model can be useful for trajectory planning, e. g. when utilizing state correlations of the model to reduce the complexity of the planner's search space. If the model is derived from human driving data, planning with such correlations means that the search space is reduced to only consider options a human would consider. Therefore, our goal is to find such correlations in human driving data to simplify the planner's search space.

We use the results of the optimization (12) of the last section, which allows further analysis of the driving behavior of humans at urban intersections. By fitting the extended bicycle model into the data, approximations of human trajectories are received. These approximations also contain information about the steering angle as well as the time-discrete actions $\boldsymbol{u}_k$ of the vehicle.

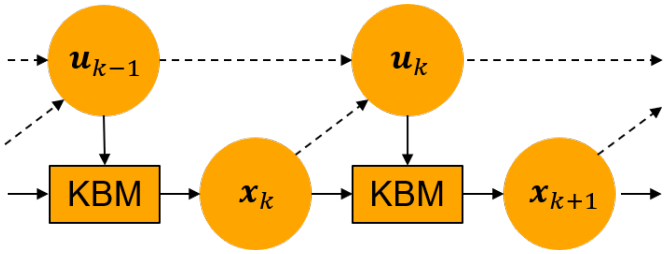

Fig. 5: Transition model of the vehicle. The next state $\boldsymbol{x}_{k+1}$ of the vehicle can be calculated according to the deterministic, extended kinematic bicycle model (KBM) of (6) to (11) (solid lines). The behavior model describes the correlations between the input $\boldsymbol{u}_k$ of the KBM dependent only on the current state $\boldsymbol{x}_k$ as well as the last input $\boldsymbol{u}_{k-1}$ (dashed lines).

Using the optimization results, the transition between the vehicle's states is defined as in the optimization by the extended kinematic bicycle model according to (6) to (11), shown in Fig. 5 as the solid lines. The input $\boldsymbol{u}_k$ is the control variable which determines the future movements of the vehicle (i. e. the next state $\boldsymbol{x}_{k+1}$) and needs to be determined by a trajectory planner. This is where the behavior model is being used: this model represents the correlations between the next input $\boldsymbol{u}_k$ and the current state $\boldsymbol{x}_k$ as well as the last chosen input $\boldsymbol{u}_{k-1}$ (dashed lines in Fig. 5). For a trajectory planner, this model can be used to focus on inputs which are human-like. For the input sampling time between two time points k and $k+1$, we choose $T_{in} = 0.6\,s$ as argued before in Sec. III.

As discussed in Sec. I, the behavior model is independent from the current traffic scenery. This means that the vehicle pose (i. e. ${}_E x_{ref}$, ${}_E y_{ref}$, ψ) and the surrounding environment (i. e.

This article has been accepted for publication in IEEE Transactions on Intelligent Transportation Systems. This is the author's version which has not been fully edited and content may change prior to final publication. Citation information: DOI: 10.1109/TITS.2022.3183204

road layout, other traffic participants, etc.) are neglected during our analysis. Hence, the state $\boldsymbol{x}$ contains only the speed v and the steering angle δ of the vehicle, whereas the input $\boldsymbol{u}$ is composed of the acceleration a and the steering rate ω of the vehicle. In a probabilistic sense, a planner is interested in the conditional probability $p(a_k, \omega_k \mid v_k, \delta_k, a_{k-1}, \omega_{k-1})$ which can be calculated through marginalization of the overall probability $p(a_k, \omega_k, v_k, \delta_k, a_{k-1}, \omega_{k-1})$. In the following, we first transform the steering variables before describing the extracted behavior model.

A. Transformation of the Steering Variables ω_k, δ_k

First, we analyze the dependencies of the vehicle's speed on the steering rate. Fig. 6 shows a 2D histogramm of the current front wheel steering rate ω_k plotted against the current speed v_k. The histogram reveals a nonlinear correlation between these two random variables. The correlation is logical, since with increasing speed the driver's steering movements become smaller to prevent greater lateral accelerations of the vehicle. This correlation can also be seen in Fig. 7, where data for two exemplarily selected speed ranges of the steering rate are shown. Here, the standard deviation for the speed range $3-4\,\mathrm{m/s}$ is 3.6 times larger compared to the speed range of $12-13\,\mathrm{m/s}$. Furthermore, it is found that within a small speed range, the data represents a Student's t distribution. For lower speeds, this t distribution approaches a normal distribution. This is conclusive because at lower speed, vehicles at intersections turn more often than at higher speeds resulting in lighter tails.

In order to appropriately describe this correlation within our behavior model, a nonlinear transformation is applied. By using the 98.0 % quantile for each speed range, we extract the exponential function

$$|\omega_{\max,k}(v_k)| = p_1\, e^{-\frac{v_k}{p_2}} \tag{18}$$

which represents the correlation between a speed $0 < v_t < 15\,\mathrm{m/s}$ and the maximum steering rate in rad/s. The values of the parameters are $p_1 = 0.6164$, $p_2 = 6.9401$ and the resulting relation is shown in Fig. 6 as the red lines. Applying the transformation

$$\overline{\omega}_k(v_k) = \frac{\omega_k}{|\omega_{\max,k}(v_k)|}, \tag{19}$$

a transformed steering rate $\overline{\omega}_k(v_k)$ is received, which is distributed equally over v_k (cf. Fig. 9a).

Similar to the steering rate ω_k, the steering angle δ_k is dependent on the speed (cf. Fig. 8). This is given by the same explanations as for ω_k. Limiting the lateral acceleration of the vehicle, a nonlinear transformation is derived by extracting the 98.0 % quantile for each speed range:

$$|\delta_{\max,k}(v_k)| = \min\left(\delta_{\max}, \arcsin\left(\frac{a_{\text{lat, max}}\, l}{v_k^2}\right)\right), \tag{20}$$

$$\overline{\delta}_k(v_k) = \frac{\delta_k}{|\delta_{\max,k}(v_k)|}, \tag{21}$$

with the maximum steering angle $\delta_{\max} = 0.44\,\mathrm{rad}$, the maximum lateral acceleration $a_{\text{lat, max}} = 2.96\,\mathrm{m/s^2}$ as well as the average wheelbase $l = 2.79\,\mathrm{m}$. For the remainder of this paper, the transformed steering rate and the transformed steering angle are used for the behavior model.

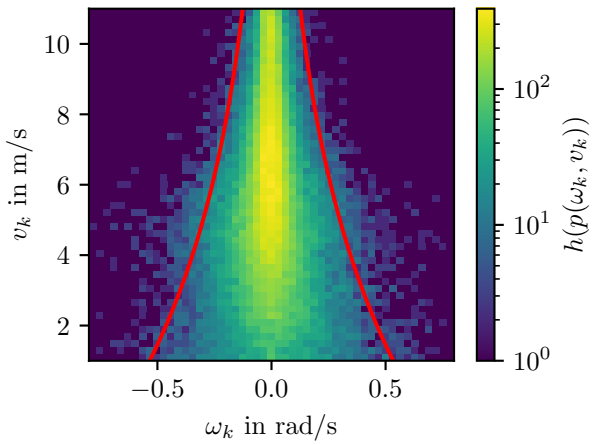

Fig. 6: 2D histogram plots of ω_k in rad/s over v_k in m/s with a logarithmic scale. For larger speeds, the absolute values of the steering rate decrease. The extracted transformation function (18) is shown in red.

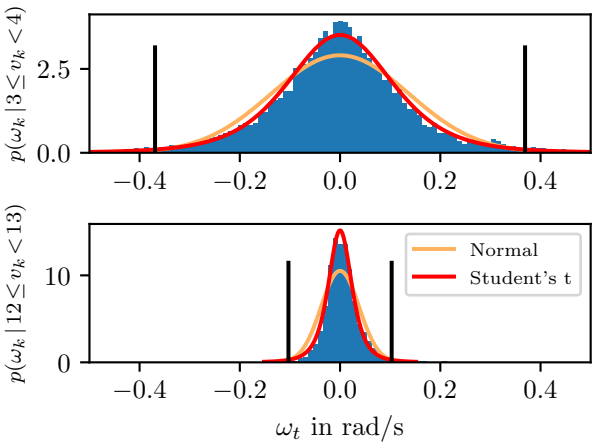

Fig. 7: Density plots of ω_k in rad/s for two different speed ranges v_k in m/s. The histogram of the ground truth data is shown in blue, a fitted normal (orange) and Student's t (red) distribution is plotted as well. The black lines limit 98.0 % of the data which is used to extract a speed dependent transformation function (18).

B. Behavior Model

After the transformation of the steering rate and angle in the previous section, the extracted behavior model is now presented. The behavior model represents the correlations between the current state $\boldsymbol{x}_k$, the last input $\boldsymbol{u}_{k-1}$ as well as the next input $\boldsymbol{u}_k$ (cf. Fig. 5). Therefore, the state vector of the model is defined as $\boldsymbol{x}_\mathrm{M} = [a_{k-1}, \overline{\omega}_{k-1}(v_{k-1}), \overline{\delta}_k(v_k), a_k, \overline{\omega}_k(v_k)]^\mathrm{T}$, whereas the speed of the vehicle is only considered indirectly through the transformations in (19) and (21). We represent the data correlations with a multivariate Gaussian distribution

$$M_\mathrm{N} = N(\boldsymbol{x}_\mathrm{M} \mid \boldsymbol{\mu}, \boldsymbol{\Sigma}) \tag{22}$$

with the vector of means $\boldsymbol{\mu}$ and the covariance matrix $\boldsymbol{\Sigma}$. Through the transformation, the nonlinearities of the steering

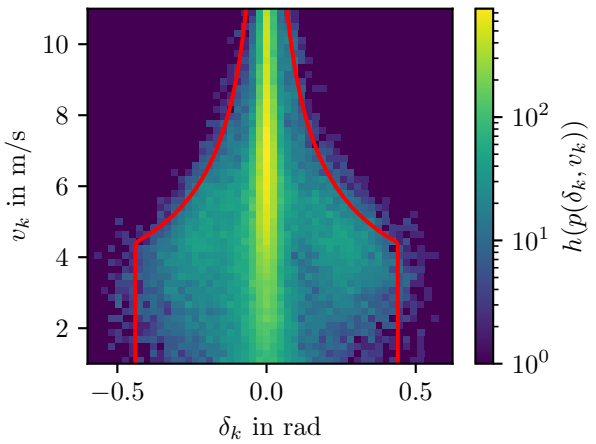

Fig. 8: 2D histogram plots of δ_k in rad over v_k in m/s with a logarithmic scale. For larger speeds, the absolute values of the steering angle decrease. The extracted transformation function (20) is shown in red.

variables are still considered even though the model consists of a multivariate Gaussian distribution.

For a trajectory planner, this model can be used for calculating the conditional probability for the next input $p(a_k, \overline{\omega}_k(v_k) \mid \overline{\delta}_k(v_k), a_{k-1}, \overline{\omega}_{k-1}(v_{k-1}))$. Then, dependent on the planning algorithm, either the remaining distribution can be used directly or possible inputs can be sampled from the distribution. In order to calculate the conditional probability, assume we have a multivariate Gaussian distribution $N(\boldsymbol{x} \mid \boldsymbol{\mu}, \boldsymbol{\Sigma})$ which can be partitioned as follows:

$$\boldsymbol{x} = \begin{bmatrix} \boldsymbol{x}_a \\ \boldsymbol{x}_b \end{bmatrix}, \quad \boldsymbol{\mu} = \begin{bmatrix} \boldsymbol{\mu}_a \\ \boldsymbol{\mu}_b \end{bmatrix}, \quad \boldsymbol{\Sigma} = \begin{bmatrix} \boldsymbol{\Sigma}_{aa} & \boldsymbol{\Sigma}_{ab} \\ \boldsymbol{\Sigma}_{ba} & \boldsymbol{\Sigma}_{bb} \end{bmatrix}. \tag{23}$$

Then, the conditional probability $p(\boldsymbol{x}_a|\boldsymbol{x}_b) = N(\boldsymbol{x} \mid \boldsymbol{\mu}_{a|b}, \boldsymbol{\Sigma}_{a|b})$ is again a Gaussian distribution and can be calculated with

$$\boldsymbol{\mu}_{a|b} = \boldsymbol{\mu}_a + \boldsymbol{\Sigma}_{ab}\boldsymbol{\Sigma}_{bb}^{-1}(\boldsymbol{x}_b - \boldsymbol{\mu}_b), \tag{24}$$

$$\boldsymbol{\Sigma}_{a|b} = \boldsymbol{\Sigma}_{aa} - \boldsymbol{\Sigma}_{ab}\boldsymbol{\Sigma}_{bb}^{-1}\boldsymbol{\Sigma}_{ba}. \tag{25}$$

The conditional probabilities of our behavior model can be calculated by only doing the matrix multiplications in (24) and (25) and the model is therefore simple and fast.

Concluding, the ingenuity of the model lies within the steering rate and angle transformations. Because of this, the vehicle's speed is only considered indirectly but the resulting data can be represented by a multivariate distribution. Through the choice of a multivariate Gaussian distribution fast marginalization and inference is possible and only a matter of matrix multiplications. Furthermore, we want to underline that the model was derived from real human driving data.

C. Model Analysis

After presenting the model in the last section we will now analyze it with regards to the given dataset. Of all the model variables $\boldsymbol{x}_\mathrm{M}$, a planner is most interested in the transformed steering rate $\overline{\omega}_k$ and the acceleration a_k. Being the control inputs of the model in Fig. 5, they define the future movement of the vehicle. Since the overall data of $\overline{\omega}_k$ and a_k represent a Student's t or approximated a Gaussian distribution, we not only fit a multivariate Gaussian M_N as in (22) into the data but also a multivariate Student's t distribution $M_\mathrm{St} = St(\boldsymbol{x} \mid \boldsymbol{\mu}, \boldsymbol{\Lambda}, \nu)$ using the expectation maximization algorithm (EM) [29].

TABLE III: Likelihood ratio $LR(M_\mathrm{N}, M_\mathrm{St})$ of the marginalized multivariate Gaussian compared to the marginalized multivariate Student's t distribution evaluated on all sample points of the dataset. The variables in the rows and columns of the table indicate the remaining variables after marginalization, similar to the plotted quantile ellipses in Fig. 9 – 10. A value larger 1 indicates that the data favors the multivariate Gaussian distribution. The overall likelihood ratio without marginalization is 3.19.

$LR(M_\mathrm{N}, M_\mathrm{St})$	$\overline{\delta}_k$	a_{k-1}	$\overline{\omega}_{k-1}$
a_k	2.76	2.73	2.74
$\overline{\omega}_k$	2.89	2.76	2.87

In Fig. 9 and 10, the 39.35 %, 86.47 % and 98.89 % quantile ellipses of the marginalized distributions are plotted as orange (Gaussian) and red (Student's t) lines. While the robust Student's t distribution focuses more on the data peaks, the orientation of the marginalized quantile ellipses can differ compared to the orientation of the Gaussian distribution (e. g. Fig. 9c) or Fig. 10d)). To compare the models, we use the likelihood ratio $LR(M_\mathrm{N}, M_\mathrm{St})$, which is 3.19. Furthermore, Tab. III shows the likelihood ratios for the plotted marginalizations of the model. A likelihood ratio larger 1 indicates that the samples of our dataset favors the Gaussian distribution. The multivariate Gaussian performs slightly better and thus, is chosen. Furthermore, the fast marginalization and inference additionally favors this simple model. We are aware that not all dependencies in the data (e. g. $\overline{\delta}_k$ on a_k) can be represented by this model, but we give greater weight to fast usability instead of an even more complex model. The parameters of the final multivariate Gaussian model M_N are

$$\boldsymbol{\mu} = \begin{bmatrix} \sigma_{a_{k-1}} \\ \sigma_{\overline{\omega}_{k-1}} \\ \sigma_{\overline{\delta}_k} \\ \sigma_{a_k} \\ \sigma_{\overline{\omega}_k} \end{bmatrix} = \begin{bmatrix} 0.0224 \\ -0.0006 \\ 0.0009 \\ -0.0109 \\ -0.0072 \end{bmatrix}, \tag{26}$$

$$\boldsymbol{\Sigma} = \begin{bmatrix} 0.8332 & 0.0249 & 0.0192 & 0.5688 & -0.0114 \\ 0.0249 & 0.0554 & 0.0170 & -0.0116 & -0.0317 \\ 0.0192 & 0.0170 & 0.0315 & 0.0026 & -0.0211 \\ 0.5688 & -0.0116 & 0.0026 & 0.8190 & 0.0235 \\ -0.0114 & -0.0317 & -0.0211 & 0.0235 & 0.0604 \end{bmatrix}. \tag{27}$$

V. Conclusion

In this paper, we analyzed human driving data at urban intersections in the context of trajectory planning. First, we analyzed the choice of input sampling time of a time-discrete, extended bicycle model with the vehicle's acceleration a and steering rate ω as inputs. By fitting the bicycle model into the human driving data, we found out that human driven trajectories can be represented with this model by an input sampling time of 0.6 s or less. Greater sampling times limit

This article has been accepted for publication in IEEE Transactions on Intelligent Transportation Systems. This is the author's version which has not been fully edited and content may change prior to final publication. Citation information: DOI: 10.1109/TITS.2022.3183204

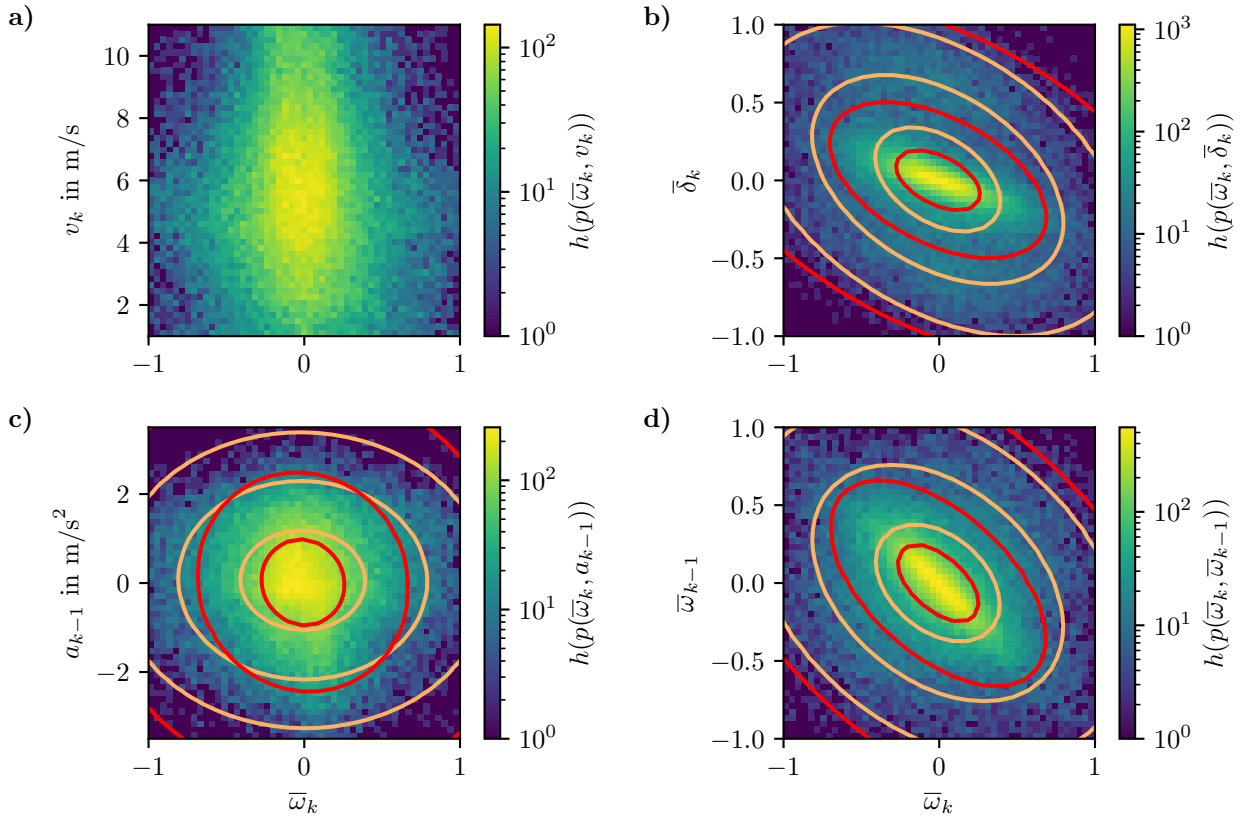

Fig. 9: Number of occurrences of the transformed front wheel steering rate $\overline{\omega}_k$ dependent on a) the current speed v_k, b) the current transformed front wheel steering angle $\overline{\delta}_k$, c) the last acceleration a_{k-1} and d) the last transformed front wheel steering rate $\overline{\omega}_{k-1}$. The lines indicates the 39.35 %, 86.47 % and 98.89 % quantile ellipses of the marginalized multivariate Gaussian (orange) and Student's t (red) distribution.

the possible movements of the vehicle so that more driven trajectories cannot be represented (cf. Tab. II).

Most trajectory planners in the literature use input sampling times of less than 0.333 s (cf. Tab. I). With our gained knowledge about the input sampling time of human driven trajectories, we want to encourage other scientists to test the use of longer sampling times in their planner. By increasing the input sampling time, the search space and therefore the complexity of the planning problem is reduced while additionally smoothening the planned trajectory. This also means less flexibility which could result in not being able to find a solution to the planning problem, but because of the analysis design as well as the presented example planner we are confident that this will not be an issue. Further advantages include the enablement of longer planning horizons and thus more efficient and foreseeing trajectories.

In a next step, we analyzed the action distributions (i. e. acceleration and front wheel steering rate) of human drivers. Here, the key points are the following: First, non-linear correlations between the lateral movement (i. e. steering angle and steering rate) and the longitudinal movement (i. e. speed) of the vehicle exist. Second, accelerations highly depend on it's previous value since the process of accelerating is longer than the sampling time. Third, while braking, the vehicle steers only slightly. These points underline the need to combine path and trajectory planning into one single step. Furthermore, speed-dependent nonlinear transformations for the steering rate and angle were introduced. In the transformed space, a transition model dependent only on the last and current time step is extracted. Here, the correlations can be modeled by a multivariate Gaussian distribution. While this model does not represent all detected data correlations, it is yet simple and can be executed fast.

For the future, we want to extend our research by analyzing the actions of human drivers dependent on the environment. In a first step, we want to incorporate the relative pose of the vehicle to the road as well as the road layout into our analysis. Since driving on roads limits the actions of human drivers, we hope to further reduce the action space of our model and therefore the planning complexity.

Furthermore, we want to integrate the gained knowledge of this publication into our trajectory planner to further reduce complexity and achieve long-term planning in urban environments.

ACKNOWLEDGMENT

We kindly thank Continental AG for their great cooperation within PRORETA 5, a joint research project of TU Darmstadt, University of Bremen, TU Iaşi and Continental AG to investigate future concepts for intelligent and learning driver assistance systems.

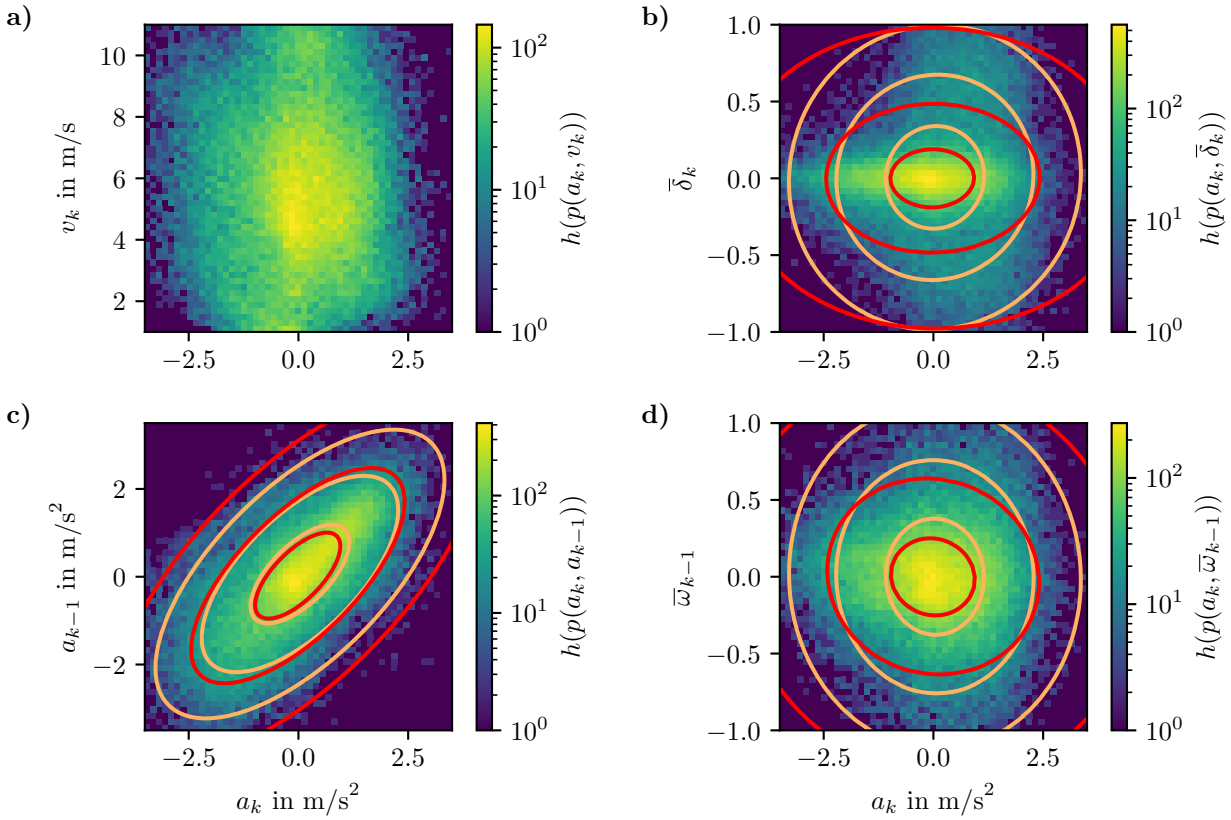

Fig. 10: Number of occurrences of the acceleration a_k dependent on a) the current speed v_k, b) the current transformed front wheel steering angle $\overline{\delta}_k$, c) the last acceleration a_{k-1} and d) the last transformed front wheel steering rate $\overline{\omega}_{k-1}$. The lines indicates the 39.35 %, 86.47 % and 98.89 % quantile ellipses of the marginalized multivariate Gaussian (orange) and Student's t (red) distribution.

References

[1] J. Bock, R. Krajewski, T. Moers, S. Runde, L. Vater, and L. Eckstein, "The inD dataset: A drone dataset of naturalistic road user trajectories at german intersections," in *2020 IEEE Intelligent Vehicles Symposium (IV)*. IEEE, oct 2020.

[2] C. M. Martinez, M. Heucke, F.-Y. Wang, B. Gao, and D. Cao, "Driving style recognition for intelligent vehicle control and advanced driver assistance: A survey," *IEEE Transactions on Intelligent Transportation Systems*, vol. 19, no. 3, pp. 666–676, mar 2018.

[3] M. Schreier, V. Willert, and J. Adamy, "Grid mapping in dynamic road environments: Classification of dynamic cell hypothesis via tracking," in *2014 IEEE International Conference on Robotics and Automation (ICRA)*. IEEE, may 2014.

[4] S. Klingelschmitt, F. Damerow, V. Willert, and J. Eggert, "Probabilistic situation assessment framework for multiple, interacting traffic participants in generic traffic scenes," in *2016 IEEE Intelligent Vehicles Symposium (IV)*. IEEE, jun 2016.

[5] Y. L. Murphey, R. Milton, and L. Kiliaris, "Driver's style classification using jerk analysis," in *2009 IEEE Workshop on Computational Intelligence in Vehicles and Vehicular Systems*. IEEE, mar 2009.

[6] M. V. Ly, S. Martin, and M. M. Trivedi, "Driver classification and driving style recognition using inertial sensors," in *2013 IEEE Intelligent Vehicles Symposium (IV)*. IEEE, jun 2013.

[7] W. Wang, J. Xi, A. Chong, and L. Li, "Driving style classification using a semisupervised support vector machine," *IEEE Transactions on Human-Machine Systems*, vol. 47, no. 5, pp. 650–660, oct 2017.

[8] P. Brombacher, J. Masino, M. Frey, and F. Gauterin, "Driving event detection and driving style classification using artificial neural networks," in *2017 IEEE International Conference on Industrial Technology (ICIT)*. IEEE, mar 2017.

[9] H. Eren, S. Makinist, E. Akin, and A. Yilmaz, "Estimating driving behavior by a smartphone," in *2012 IEEE Intelligent Vehicles Symposium*. IEEE, jun 2012.

[10] D. Yokoyama and M. Toyoda, "Do drivers' behaviors reflect their past driving histories? - large scale examination of vehicle recorder data," in *2016 IEEE International Congress on Big Data (BigData Congress)*. IEEE, jun 2016.

[11] F. Damerow and J. Eggert, "Risk-aversive behavior planning under multiple situations with uncertainty," in *2015 IEEE 18th International Conference on Intelligent Transportation Systems*. IEEE, sep 2015.

[12] X. He, D. Xu, H. Zhao, M. Moze, F. Aioun, and F. Guillemard, "A human-like trajectory planning method by learning from naturalistic driving data," in *2018 IEEE Intelligent Vehicles Symposium (IV)*. IEEE, jun 2018.

[13] A. Sadat, M. Ren, A. Pokrovsky, Y.-C. Lin, E. Yumer, and R. Urtasun, "Jointly learnable behavior and trajectory planning for self-driving vehicles," in *2019 IEEE/RSJ International Conference on Intelligent Robots and Systems (IROS)*. IEEE, nov 2019.

[14] J. Reif and M. Sharir, "Motion planning in the presence of moving obstacles," in *26th Annual Symposium on Foundations of Computer Science (sfcs 1985)*. IEEE, 1985.

[15] B. Paden, M. Cap, S. Z. Yong, D. Yershov, and E. Frazzoli, "A survey of motion planning and control techniques for self-driving urban vehicles," *IEEE Transactions on Intelligent Vehicles*, vol. 1, no. 1, pp. 33–55, mar 2016.

[16] P. Bokare and A. Maurya, "Acceleration-deceleration behaviour of various vehicle types," *Transportation Research Procedia*, vol. 25, pp. 4733–4749, 2017.

[17] C. Miyajima, Y. Nishiwaki, K. Ozawa, T. Wakita, K. Itou, K. Takeda, and F. Itakura, "Driver modeling based on driving behavior and its evaluation in driver identification," *Proceedings of the IEEE*, vol. 95, no. 2, pp. 427–437, feb 2007.

[18] P. Wagner, R. Nippold, S. Gabloner, and M. Margreiter, "Analyzing human driving data an approach motivated by data science methods," *Chaos, Solitons & Fractals*, vol. 90, pp. 37–45, sep 2016.

[19] C. Miyajima, H. Ukai, A. Naito, H. Amata, N. Kitaoka, and K. Takeda, "Driver risk evaluation based on acceleration, deceleration, and steering

behavior," in *2011 IEEE International Conference on Acoustics, Speech and Signal Processing (ICASSP)*. IEEE, may 2011.
[20] J. Strohbeck, V. Belagiannis, J. Muller, M. Schreiber, M. Herrmann, D. Wolf, and M. Buchholz, "Multiple trajectory prediction with deep temporal and spatial convolutional neural networks," in *2020 IEEE/RSJ International Conference on Intelligent Robots and Systems (IROS)*. IEEE, oct 2020.
[21] J. Schulz, C. Hubmann, N. Morin, J. Lochner, and D. Burschka, "Learning interaction-aware probabilistic driver behavior models from urban scenarios," in *2019 IEEE Intelligent Vehicles Symposium (IV)*. IEEE, jun 2019.
[22] J. Kong, M. Pfeiffer, G. Schildbach, and F. Borrelli, "Kinematic and dynamic vehicle models for autonomous driving control design," in *2015 IEEE Intelligent Vehicles Symposium (IV)*. IEEE, jun 2015.
[23] F. Seccamonte, J. Kabzan, and E. Frazzoli, "On maximizing lateral clearance of an autonomous vehicle in urban environments," in *2019 IEEE Intelligent Transportation Systems Conference (ITSC)*. IEEE, oct 2019.
[24] P. Polack, F. Altche, B. d'Andrea Novel, and A. de La Fortelle, "The kinematic bicycle model: A consistent model for planning feasible trajectories for autonomous vehicles?" in *2017 IEEE Intelligent Vehicles Symposium (IV)*. IEEE, jun 2017.
[25] J. A. Matute, M. Marcano, S. Diaz, and J. Perez, "Experimental validation of a kinematic bicycle model predictive control with lateral acceleration consideration," *IFAC-PapersOnLine*, vol. 52, no. 8, pp. 289–294, 2019.
[26] S. Dixit, U. Montanaro, M. Dianati, D. Oxtoby, T. Mizutani, A. Mouzakitis, and S. Fallah, "Trajectory planning for autonomous high-speed overtaking in structured environments using robust MPC," *IEEE Transactions on Intelligent Transportation Systems*, vol. 21, no. 6, pp. 2310–2323, jun 2020.
[27] B. Gutjahr, L. Groll, and M. Werling, "Lateral vehicle trajectory optimization using constrained linear time-varying MPC," *IEEE Transactions on Intelligent Transportation Systems*, pp. 1–10, 2016.
[28] J. Ziegler, P. Bender, T. Dang, and C. Stiller, "Trajectory planning for bertha - a local, continuous method," in *2014 IEEE Intelligent Vehicles Symposium Proceedings*. IEEE, jun 2014.
[29] A. P. Dempster, N. M. Laird, and D. B. Rubin, "Maximum likelihood from incomplete data via the em algorithm," *Journal of the Royal Statistical Society: Series B (Methodological)*, vol. 39, no. 1, pp. 1–22, sep 1977.

Christoph Ziegler received the B.S. and M.S. degrees in electrical engineering and information technology from Technical University of Darmstadt, Germany in 2015 and 2017 respectively. During and after his studies he worked in a startup on printing machines for printed electronics before coming back to university. Since 2019 he is a research associate with the Control Methods and Robotics Lab and working towards his Ph.D. degree. His research interests include the analysis of human driving data and trajectory planning.

Volker Willert received the Dipl.-Ing. degree in electrical engineering and information technology and the Dr.-Ing. degree in control theory and robotics, with a focus on dynamical computer vision, from Technical University of Darmstadt, Germany, in 2002 and 2006, respectively. From 2005 to 2009, he was a Senior Scientist at Honda Research Institute Europe GmbH, and from 2009 to 2020, he has been with the Chair of the Control Methods and Robotics Laboratory, TU Darmstadt. As an Akademischer Oberrat and lecturer, he lead the research group Machine Vision and Mobile Robotics. Since 2020, he has been a professor at the University of Applied Sciences Würzburg-Schweinfurt, Germany. His main research interests are in the fields of machine intelligence, computer vision, distributed controls, and machine learning for mobile robotics, multiagent systems, and driver assistance systems.

Jürgen Adamy received his Diploma in engineering degree in electrical engineering in 1987 and Ph.D. degree in control theory in 1991 from the University of Dortmund, Germany. From 1991 to 1995 he worked as a research engineer, and from 1995 to 1998 as a research manager, at the Siemens Research Center at Erlangen, Germany. Since 1998 he has been a professor at the Technical University of Darmstadt, Germany, and head of its Control Methods and Robotics Laboratory. His main fields of research are control theory, computational intelligence and autonomous mobile robots.